# Solution Dynamics of p21$^{ras}$ Proteins Bound with Fluorescent Nucleotides: A Time-Resolved Fluorescence Study†

Theodore L. Hazlett,*,‡ Keith J. M. Moore,§ Peter N. Lowe,∥ David M. Jameson,⊥ and John F. Eccleston§

*Laboratory for Fluorescence Dynamics, Department of Physics, University of Illinois at Urbana-Champaign, 1110 West Green Street, Urbana, Illinois 61801, National Institute for Medical Research, Mill Hill, London NW7 1AA, United Kingdom, Department of Cell Biology, Wellcome Research Laboratories, Langley Court, Beckenham, Kent BR3 3BS, United Kingdom, and Department of Biochemistry and Biophysics, University of Hawaii at Manoa, 1960 East West Road, Honolulu, Hawaii 96815*

*Received July 15, 1993; Revised Manuscript Received September 21, 1993*®

ABSTRACT: The solution dynamics of normal and transforming p21$^{ras}$ proteins in both the GTP- and GDP-bound forms were examined with time-resolved fluorescence spectroscopy. The fluorescent 2′(3′)-*O*-(*N*-methylanthraniloyl) derivatives (mant derivatives) of GTP, dGTP, and GDP and the aminocoumarin and fluorescein derivatives of GTP and GDP were synthesized and used as reporter groups. The fluorescence lifetimes at 5 °C of the mant nucleotide derivatives increased from approximately 4 ns in solution to approximately 9 ns when bound to p21$^{ras}$. At 30 °C, there was a 7.8% difference in lifetime between normal p21$^{ras}$·mantGTP and p21$^{ras}$·mantGDP, but no difference between similar complexes of the [Asp-12]p21$^{ras}$ protein. These data are consistent with steady-state fluorescence intensity differences among p21$^{ras}$·mantGTP, p21$^{ras}$·mantGDP, and the free nucleotides. Rotational correlation times for the mantGTP- and mantGDP-bound p21 proteins, *N-ras*, *K-ras*, and *H-ras*, were similar at 26 ns (5 °C), which is significantly longer than the 15-ns rotational correlation time predicted for a globular 21 000-Da protein. The p21-bound fluorescein and aminocoumarin nucleotide derivatives reported correlation times of 19 and 29 ns, respectively. Global analysis of the three fluorophore·p21 complexes with linked protein rotational correlation functions were best fit with a common rotational correlation time of 28 ns. Gel permeation chromatography of the GDP and mantGDP complexes of normal p21$^{N\text{-}ras}$ also showed greater apparent molecular weights than were expected in both cases, demonstrating that the high rotational correlation times obtained from time-resolved fluorescence measurements were not a result of the introduction of the fluorophore. The rotational data are discussed in terms of two mutually exclusive hypotheses: the p21 proteins are dimeric, or they are monomeric with an extended, asymmetric shape.

The products of *N*-, *K*-, and *H-ras* genes, termed p21$^{ras}$,[1] are 21-kDa proteins that bind GTP and GDP tightly and have a low intrinsic GTPase activity [for reviews, see Barbacid (1987) and Bourne et al. (1990)]. Single amino acid substitutions at specific positions in the molecule, or overexpression of the normal proteins, cause transforming effects, with approximately 30% of human tumors containing such activated p21$^{ras}$ proteins. These proteins act as switches in a biological signal transduction pathway, controlling DNA synthesis and cell division. The ras family of proteins forms part of a superfamily of proteins based on sequence homology, the other two families being the rho family and the rab family. The rho family is thought to be involved in the organization of the cytoskeleton and the rab family in the secretory pathways (Hall, 1990).

The first 166 residues constitute the guanine nucleotide binding domain and show a high degree of sequence similarity in all three p21$^{ras}$ protein products. The three mammalian ras genes differ significantly in their 23 C-terminal amino acids. This region is posttranslationally modified in mammalian cells and is required for association with the plasma membrane. Recombinant proteins expressed in *Escherichia coli* do not contain these posttranslational modifications. Truncation of the protein to remove the 23 C-terminal amino acids does not affect the guanine nucleotide binding properties of the H-ras or K-ras proteins (John et al., 1989; Lowe et al., 1991).

The tertiary structure of p21$^{H\text{-}ras}$ has been determined to high resolution by X-ray diffraction studies. These crystal structures have been obtained with recombinant proteins which have been truncated at position 166. Structures have been reported on a variety of truncated p21·nucleotide complexes: p21·GTP, p21·Gpp[NH]p, p21·Gpp[$CH_2$]P, p21·caged GTP, and p21·GDP (Tong et al., 1989, 1990; Milburn et al., 1990; Pai et al., 1990; Schlichting et al., 1990a; Wittinghofer et al., 1991). The major difference between the triphosphate (and triphosphate-like) form and the diphosphate form of the p21 proteins occurs in the amino acids between Tyr-32 and Ile-36. These residues form part of the loop which has been defined by mutagenesis studies to be essential for interaction of the p21$^{ras}$ proteins with their target effector proteins and the GTPase-activating proteins or GAPs. Structural shifts are also observed in the region of residues 58–65, although the differences between the forms are less well defined due to the

† This work was supported in part by NSF Grant DMB 9005195, the Medical Research Council (United Kingdom), NIH Grant RR03155, and the Human Frontier Science Program. D.M.J. is an Established Investigator of the American Heart Association.

* Author to whom correspondence should be addressed.
‡ University of Illinois at Urbana–Champaign.
§ National Institute for Medical Research.
∥ Wellcome Research Laboratories.
⊥ University of Hawaii at Manoa.

® Abstract published in *Advance ACS Abstracts,* November 1, 1993.

[1] Abbreviations: p21, the p21 protein product of the *N-ras* gene unless otherwise stated; Gpp[NH]p, guanosine 5′-($\beta\gamma$-imido triphosphate); mantGTP, 2′(3′)-*O*-(*N*-methylanthraniloyl)guanosine 5′-triphosphate; corresponding mant derivatives of GDP, dGTP, and Gpp[NH]p are abbreviated similarly.

0006-2960/93/0432-13575$04.00/0 

diffuse electron density of this region. The structures of some oncogenic mutant proteins have been determined, but show only small ill-defined differences in this latter region.

In contrast to the detailed tertiary structural information, the quaternary structure of the ras protein has not been extensively studied, and it is often assumed to be a monomeric protein. However, a few experiments have addressed this issue. Radiation inactivation studies have been carried out on $p21^{H\text{-}ras}$ both in membranes and in bacterial-expressed purified protein (Santos et al., 1988). In both cases, the results gave a target size consistent with the protein being a dimer or trimer. The presence of high concentrations of dithiothreitol gave identical results, thus excluding the possibility of dimers via formation of intermolecular disulfide bonds. Other workers have also reported evidence for $p21^{H\text{-}ras}$ aggregation (John et al., 1989). Gel permeation chromatography of full-length $p21^{H\text{-}ras}$ gave an apparent molecular mass 20% larger than expected of a 21-kDa protein, although the truncated protein (containing residues 1–166) gave the predicted molecular mass of 18.5 kDa. This observation suggests that the C-terminal tail is involved in the oligomerization process. Takai and co-workers have used gel permeation chromatography and sucrose gradient centrifugation to study the oligomerization of the closely related proteins smg25A (also known as Rab3), smg21A (also known as Rap1A and Krev-1), and smg21B and rhoB (Ueda et al., 1990; Arakai et al., 1990; Mizuno et al., 1991; Kawamura et al., 1991). The results clearly indicated that these proteins were dimeric or trimeric homooligomers.

Fluorescence parameters of fluorophores bound to particular protein domains can give a variety of data on local structural and conformational changes upon system perturbations. Fluorescence lifetimes in particular contain information on the dynamic interactions of the probe with its environment. In light of the steady-state work already published on the $p21^{ras}$·mant nucleotide complexes (Neal et al., 1990; Rensland et al., 1991; Eccleston et al., 1991), time-resolved fluorescence lifetime measurements were made to further characterize conformational differences in the GTP and GDP protein forms and to monitor the dynamics of the nucleotide site.

In the work reported here, we have made time-resolved fluorescence lifetime measurements to examine the local region of the p21 nucleotide binding domain and, through dynamic polarization studies, have characterized the rotational correlation times of the $p21^{N\text{-}ras}$, $p21^{K\text{-}ras}$, and $p21^{H\text{-}ras}$ complexes with the mant, fluorescein, and aminocoumarin analogues of GTP and GDP. In all complexes examined, the rotational correlation times measured were significantly longer than that expected for a spherical, monomeric $p21^{ras}$ protein. These data are consistent with the hypothesis that the $p21^{ras}$ proteins either are dimeric in solution or have an asymmetric shape not indicated by the published crystal structures of the truncated proteins.

## MATERIALS AND METHODS

*Proteins.* Normal and oncogenic mutants were expressed and purified as described by Hall and Self (1986) for $p21^{N\text{-}ras}$ and $p21^{H\text{-}ras}$ and by Lowe et al. (1991) for $p21^{K\text{-}ras}$.

*Nucleotides.* mantGTP and mantGDP were synthesized by the method of Hiratsuka (1983) and purified and characterized as previously described (Neal et al., 1990). Other fluorescent nucleotides were synthesized by methods based on work on adenine nucleotides (Cremo et al., 1990). This synthesis involves the formation of the 2′,3′-cyclic carbonate derivative of the nucleotide (Maeda et al., 1977) followed by the reaction with an amine to give the 2′(3′)-carbamate derivative. The trisodium salt of GTP (520 μmol) was applied to a DE-52 column in the bicarbonate form, and after washing with water it was eluted with 0.6 M triethylammonium bicarbonate as the triethylammonium salt and evaporated to dryness. Triethylammonium bicarbonate was removed by successive (3×) additions of methanol and evaporations *in vacuo*. Tributylamine (0.48 mL, 2 mmol) was then added and the nucleotide made anhydrous by repeated (3×) additions and evaporations of dry dimethylformamide. The nucleotide was dissolved in 8 mL of dry dimethylformamide to which 405 mg (2.5 mmol) of *N,N′*-carbonyldiimidazole was added. The solution was then stirred for 6 h at 4 °C, and the remaining excess *N,N′*-carbonyldiimidazole was removed by the addition of 144 μL (3.6 mmol) of methanol. Ethylenediamine (167 μmol in 5 mL of dry dimethylformamide) was added dropwise to this solution. The white precipitate was recovered by centrifugation, washed three times with dry dimethylformamide, dissolved in 30 mL of water, adjusted to a pH of 2.5 with HCl, and left for 16 h at 4 °C. HPLC analysis on a Whatman SAX column (4 mm × 30 cm) eluting with 0.6 M ammonium phosphate (pH 4.0) showed that the ethylenediamine derivative of GTP had been formed at a yield of 60%. The mixture was purified over a DE-52 column (4 × 30 cm) in the bicarbonate form and eluted with a 3-L linear gradient of 10 to 600 mM triethylammonium bicarbonate (pH 7.6). The 5′-diphosphate derivative was prepared by hydrolysis of the 5′-triphosphate analogue with myosin subfragment 1 in 20 mM Tris (pH 7.5) and 5 mM EDTA. The reaction was monitored by the HPLC system described above, and the product was purified in the same way as the 5′-triphosphate.

The fluorescein derivatives of GTP and GDP were prepared by the reaction of 1 mM 2′(3′)-*O*-ethylenediamine GTP or GDP in 20 mM sodium bicarbonate with an equal volume of 5 mM fluorescein isothiocyanate (isomer I, Molecular Probes, Inc.) in acetone. The reaction was allowed to proceed at room temperature for 3 h. TLC analysis of both the 5′-diphosphate and 5′-triphosphate on Merck silica gel 60 F254 eluted with isopropyl alcohol/water/ammonium hydroxide (70:20:10) showed the formation of a new fluorescent species which remained at the origin. The products were then purified on a DE-52 bicarbonate column as described above. Analysis of the products by Merck silica gel 60 F254 TLC plates eluted with isopropyl alcohol/water/ammonium hydroxide (70:20:30) showed pure compounds with $R_f$ values for the tri- and diphosphate derivatives of 0.28 and 0.44, respectively. Treatment of the 5′-triphosphate form with myosin subfragment 1 resulted in the conversion to a spot with a mobility identical to that of the 5′-diphosphate.

Preparation of the aminocoumarin GTP derivative was carried out in a manner similar to the fluorescein derivative, with one exception: a 5-fold excess of aminocoumarin (Corrie, 1990) was reacted directly with the 2′,3′-cyclic carbonate of GTP in dry dimethylformamide and allowed to react for 3 days at 20 °C. Thin-layer chromatography analysis and column purification of the aminocoumarin GTP derivative were as described for the fluorescein analogue. The structures of the three fluorescent nucleotide derivatives are shown in Figure 1.

*Preparation of Nucleotide·$p21^{ras}$ Complexes.* Complexes of $p21^{ras}$ with fluorescent nucleotides were made either with the apoprotein obtained from hydrophobic interaction chromatography (Feuerstein et al., 1987; Neal et al., 1990) or by direct exchange of nucleotide. For the latter method, a 20-fold molar excess of analogue was added to p21ras·GDP in 50 mM Tris-HCl (pH 7.5), 20 mM EDTA, and 200 mM

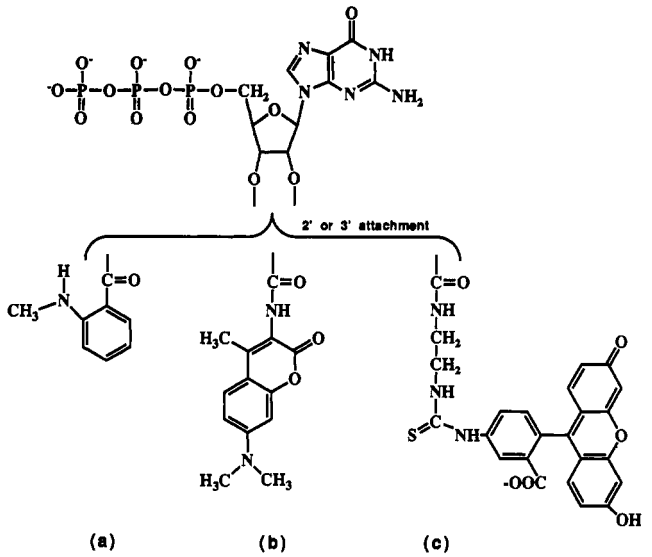


FIGURE 1: Structure of GTP and the three fluorescent probes [mant (a), aminocoumarin (b), and fluorescein (c)] used in this study. The probes were attached to a single ribose hydroxyl group, either 2′ or 3′, of GTP, GDP, and dGTP via an ester or a carbamate linkage.

ammonium sulfate and incubated for 10 min at 20 °C. In both cases, the protein·nucleotide complexes were separated from excess free nucleotide by gel filtration on PD-10 desalting columns (Pharmacia) preequilibrated in 50 mM Tris-HCl (pH 7.5), 50 mM NaCl, 10 mM $MgCl_2$, and 10 mM dithiothreitol. Similar complexes prepared by each of the two protocols were indistinguishable as to GTP binding and intrinsic GTPase activity. Concentrations of the complex were based on the absorption of the fluorophore: mant, $\epsilon_{350} = 5\,700$ $cm^{-1}$ $M^{-1}$ (Hiratsuka, 1983); fluorescein, $\epsilon_{495} = 75\,000$ $cm^{-1}$ $M^{-1}$ (Chen, 1969); and aminocoumarin, $\epsilon_{371} = 24\,800$ $cm^{-1}$ $M^{-1}$ (Corrie, 1990). Unless specifically stated, the concentrations used in the fluorescence measurements were between 1 and 15 $\mu$M. The resolved lifetimes and rotational correlation times of all complexes studied were invariant through this protein concentration range.

*Analytical Gel Permeation Chromatography.* Gel permeation chromatography was carried out on a 66.5 × 1.6 cm ACA-54 column (Pharmacia-LKB, Inc.) equilibrated and eluted at 25 °C in 50 mM Tris-HCl (pH 7.5), 100 mM NaCl, and 10 mM $MgCl_2$. The column was run at a constant flow rate of approximately 12 mL/h. The protein standards used to calibrate the columns and their molecular masses were as follows: aprotinin, 6.5 kDa; cytochrome C, 12 kDa; carbonic anhydrase, 29 kDa; horse radish peroxidase, 45 kDa; and bovine serum albumin, 66 kDa. The volumes and concentrations loaded onto the ACA-54 gel of p21$^{N\text{-}ras}$·mantGDP and p21$^{N\text{-}ras}$·GDP were 1.7 mL at 22 $\mu$M and 1 mL at 15 $\mu$M, respectively. Both proteins elute at a volume of 84 mL, corresponding to a molecular mass of 27 kDa.

*Fluorescence Measurements.* Fluorescence spectra and polarization were measured with an SLM (Urbana, IL) Model 8000 photon-counting spectrofluorometer equipped with Glan-Thompson prism polarizers or with an I.S.S. Greg PC photon-counting fluorometer, also equipped with prism polarizers. Excitation of the fluorescein, mant, and coumarin probes was at 480, 350, and 370 nm, respectively.

Time-resolved fluorescence data were taken on either a home-built multifrequency phase and modulation fluorometer based on the Gratton design (Gratton & Limkeman, 1983) or an ISS K2 instrument (ISS Inc., Champaign, IL). Excitation of the mant, aminocoumarin, and fluorescein nucleotide derivatives was accomplished using the 351-, 364-, and 488-nm lines, respectively, of a SpectraPhysics Model 2025 or Model 2045 argon ion laser. The emission of the mant- and aminocoumarin-labeled nucleotides was observed through both a Schott KV 399 and a Schott GG 420 cutoff filter; the fluorescein-labeled nucleotide was observed through a single Schott OG 530-nm cutoff filter. To eliminate any polarization artifacts in the lifetime measurements the excitation beam was routinely polarized normal to the laboratory plane, 0°, and the emission was observed at the magic angle, 55° (Spencer & Weber, 1970).

In the multifrequency phase and modulation approach, fluorescence lifetimes, $\tau$, are determined by modulating the excitation light and measuring the phase shift between the excitation, or known fluorescence standard, and the fluorescence of the sample (Spencer & Weber, 1969). For the aminocoumarin and mant fluorophores, either glycogen (scatter, $\tau = 0$ ns) or dimethyl-POPOP ($\tau = 1.43$ ns) was used as the reference compound. Fluorescein in 0.1 M NaOH ($\tau = 4.05$ ns) was used as the reference for fluorescein-labeled nucleotide. Fluorescence lifetimes are described by a single decay for a homogeneous system or by multiexponential decay for heterogeneous systems. Fluorescence decays collected in the frequency domain are the Fourier transform of the decay in the time domain (Spencer & Weber, 1969; Weber, 1981). In the time domain, the decay is given by the following equation:

$$I(t) = I_0 \sum_i \alpha_i e^{-t/\tau_i} \tag{1}$$

where $I(t)$ is the change of intensity with time, $I_0$ is the is the intensity at time 0, $\alpha_i$ is the preexponential factor for the $i$th lifetime component, $t$ is time, and $\tau_i$ is the $i$th lifetime.

Fluorescence lifetimes taken by the phase and modulation method use an intensity-modulated excitation beam, which results in a modulated fluorescence emission. The sample lifetime(s) is(are) then determined by the relative phase shift and demodulation of the fluorescence with respect to the excitation beam or a known fluorescence standard. Phase and modulation lifetimes at a given modulation frequency are then calculated by the following equations (Spencer & Weber, 1969; Weber, 1981):

$$\tan P = \omega \tau_p \tag{2}$$

$$M = [1 + (\omega \tau_m)^2]^{-1/2} \tag{3}$$

where $P$ is the phase shift, $M$ is the relative modulation, and $\omega$ is the angular modulation frequency. In heterogeneous systems, these two apparent lifetimes, $\tau_p$ and $\tau_m$, will yield different values, depending on the modulation frequency, which will affect the weighting of short and long components, the fluorescent lifetimes, and their fractional intensities.

By collecting data over a range of modulation frequencies and fitting to the entire phase and modulation data set, the lifetimes, and their respective fractional intensities, of a complex system can be extracted. The data are fit to single- or multiexponential decay models using nonlinear least-squares analysis procedures. The goodness of the fit was judged by the reduced $\chi^2$ (Gratton et al., 1984; Jameson et al., 1984), defined as

$$\chi^2 = \sum \{[(P_c - P_e)/\sigma_p] + [(M_c - M_e)/\sigma_m]\}^2/(2n - f - 1) \tag{4}$$

where $n$ is the number of modulation frequencies and $f$ is the

number of free parameters. $P$ and $M$ correspond to the phase shift and relative modulation values, respectively, and the indices c and e indicate the calculated and experimental values. The variables $\sigma_p$ and $\sigma_m$ are the standard deviation of each phase and modulation measurement, respectively. Unless otherwise stated, the analyses were performed using constant standard deviations of 0.2° for the phase shift and 0.004 for the modulation. Data analysis was performed using either software available from ISS Inc. (Champaign, IL) or the Globals Unlimited software (Laboratory for Fluorescence Dynamics, Department of Physics, University of Illinois, Urbana, IL).

The rotational correlation times of the probes and the probes bound to p21$^{ras}$ are derived from dynamic polarization measurements. In this method, the phase delay between the parallel and perpendicular emission components is determined along with the relative modulation of the these components. The observed phase delays and modulation ratios depend upon the modulation frequency and the rotational rates of the sample. The decay of anisotropy, as measured in the time domain, is reflected in the collected phase and modulation data. Data are taken over a wide frequency range which, similar to the lifetime experiment, will differentially weight the fast and slow rotational modes. The results are then normally analyzed with single- and multiexponential models. The goodness of the fit is judged by a reduced $\chi 2$ similar in form to eq 4. Further details on the analysis of the multifrequency phase and modulation data are given elsewhere (Weber, 1977; Gratton et al., 1984; Jameson & Hazlett, 1991). For brevity, only the time domain equation is given:

$$r(t) = r_0 \sum_i \alpha_i e^{-t/\tau_{ci}} \qquad (5)$$

where $r(t)$ is the anisotropy at time $t$, $r_0$ is the limiting anisotropy, $\alpha_i$ is the preexponential factor of the $i$th rotational component, and $\tau_{ci}$ is the rotational correlation time of the $i$th component.

## RESULTS

*Fluorescence Lifetimes.* The 2′ or 3′ position of the guanine nucleotide ribose ring was covalently labeled with the fluorescent mant group. The 2′ and 3′ isomers have been shown to establish a 40:60 2′:3′ equilibrium in aqueous buffers at neutral pH (Cremo et al., 1990; Rensland et al., 1991; Eccleston et al., 1991). The mant 3′ isomer preferentially binds the p21$^{ras}$ proteins, representing 80–90% of the bound mant nucleotide (Rensland et al., 1991; Eccleston et al., 1991). The GTP and GDP forms of the mant nucleotide were synthesized, as well as the 2′-deoxyGTP (dGTP) form which is labeled only at the 3′ position. Representative phase and modulation lifetime data and the best-fit curves for mantdGTP and p21$^{N\text{-}ras}$·mantdGTP are shown in Figure 2. A scattering component, assigned as a 1-ps fluorescence lifetime, was routinely fixed in the analyses to correct for scattered light (Rayleigh or Raman) incompletely removed by the cutoff filters. The absence of significant amounts of free nucleotide in the samples was confirmed by the lifetime data, i.e., the absence of a 4.1-ns component, and also it is unlikely since the concentrations of p21$^{ras}$ and mant nucleotide complexes were greater than 1 $\mu$M, exceeding the estimated $K_d$ of $10^{-11}$ M by 5 orders of magnitude (John et al., 1990; Neal et al., 1990). Since there was no significant difference between mantGTP and mantdGTP, whether free or protein-bound, all subsequent experiments were performed with the mant guanosine derivatives.

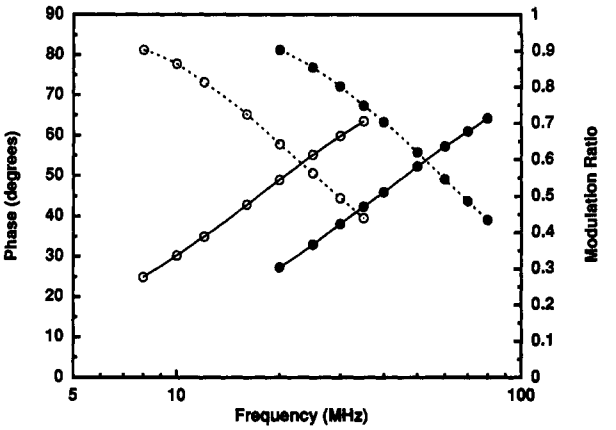


FIGURE 2: Lifetime multifrequency phase (—) and modulation data (- - -) for mantdGTP (●) and p21$^{N\text{-}ras}$·mantdGTP (○) at 5 °C. Samples were excited with the 351-nm line of an argon ion laser, and emission was measured through Schott GG 420 and KV 399 cutoff filters. The curves represent the least-squares best fits to the data points. The resolved fluorescence lifetimes for the free and bound fluorophores were 4.1 and 9.2 ns, respectively.

Table I: Fluorescence Lifetime Parameters (5 °C)

| sample[a] | $\tau$ (ns)[b] | $\chi^2$ |
|---|---|---|
| mantGDP | 4.13 ± 0.02 | 2.0 |
| mantGTP | 4.22 ± 0.02 | 2.1 |
| mantdGTP | 4.10 ± 0.02 | 3.1 |
| p21$^{N\text{-}ras}$·mantGDP | 9.03 ± 0.01 | 1.1 |
| [Asp$^{12}$]p21$^{N\text{-}ras}$·mantGDP | 9.07 ± 0.04 | 1.4 |
| p21$^{H\text{-}ras}$·mantGDP | 8.5 ± 0.1 | 5.9 |
| p21$^{K\text{-}ras}$·mantGDP | 8.4 ± 0.2 | 9.6 |
| p21$^{N\text{-}ras}$·mantGTP | 9.25 ± 0.03 | 1.6 |
| [Asp$^{12}$]p21$^{N\text{-}ras}$·mantGTP | 9.23 ● 0.03 | 1.1 |
| p21$^{N\text{-}ras}$·mantdGTP | 9.21 ± 0.04 | 1.3 |

[a] Representative data sets are shown for the p21$^{N\text{-}ras}$ samples, while the p21$^{H\text{-}ras}$ and p21$^{K\text{-}ras}$ data are the result of the average of three separate sets. [b] A scattering component, modeled as a 0.001-ns lifetime, was routinely fixed in the analysis.

A summary of the fluorescence lifetimes for the free and bound nucleotide analogues is given in Table I. All of the nucleotides (mantGTP, mantdGTP, and mantGDP) in aqueous buffer gave lifetimes of approximately 4.1 ns. Upon binding to normal p21$^{N\text{-}ras}$, the mantGTP, mantdGTP, and mantGDP nucleotide lifetimes increased to 9.2, 9.2, and 9.0 ns, respectively. The small difference in the lifetimes of p21$^{N\text{-}ras}$·mantGTP and p21$^{N\text{-}ras}$·mantGDP (5 °C) was unexpected considering the 10% difference in the fluorescence steady-state intensity of the two complexes for the normal protein reported at 37 °C (Neal et al., 1990). The effect of temperature on the lifetimes of mantGTP and mantGDP bound to the normal and to the [Asp-12]p21$^{N\text{-}ras}$ proteins was examined to resolve this apparent discrepancy. To minimize the p21 hydrolysis of mantGTP, the lifetime data were collected in under 5 min through the use of digital data acquisition technology and Fast Scan software (ISS Inc., Champaign, Illinois). The values obtained are given in Table II.

The lifetimes for all complexes showed a decrease in value with increasing temperature. However, the effect is less pronounced with normal p21$^{N\text{-}ras}$·mantGTP than with the other three complexes studied. At 30 °C there is now a 7.8% difference between the bound p21·mantGTP and p21·mantGDP complexes. This difference in lifetime would be expected to increase at 37 °C and match the previously reported steady-state data reasonably well. The correlation between the steady-state and lifetime measurements is confirmed by data in which the lifetime of p21$^{N\text{-}ras}$·mantGTP was measured

Table II: Temperature Dependence Fluorescence Lifetimes

| sample[a] | temp (°C) | $\tau$ (ns)[b] | $\chi^2$ |
|---|---|---|---|
| p21$^{N\text{-}ras}$·mantGDP | 30.0 | 7.6 ± 0.1 | 2.0 |
| | 20.6 | 8.4 ± 0.1 | 2.7 |
| | 10.7 | 9.0 ± 0.1 | 3.6 |
| | 4.9 | 9.2 ± 0.1 | 3.4 |
| p21$^{N\text{-}ras}$·mantGTP | 30.3 | 8.2 ± 0.1 | 1.9 |
| | 5.0 | 9.3 ± 0.1 | 1.6 |
| [Asp12]p21$^{N\text{-}ras}$·mantGDP | 30.0 | 7.7 ± 0.1 | 3.7 |
| | 20.6 | 8.2 ± 0.1 | 2.4 |
| | 5.0 | 9.1 ± 0.1 | 1.4 |
| [Asp12]p21$^{N\text{-}ras}$·mantGTP | 30.0 | 7.8 ± 0.1 | 5.1 |
| | 20.6 | 8.3 ± 0.1 | 2.0 |
| | 5 | 9.2 ± 0.1 | 1.1 |

[a] Temperature was regulated within 0.2 °C and measured in a companion cell placed in the turret. [b] A scattering component, 0.001 ns, was routinely fixed in the analysis and represented no more than 2% of the signal.

throughout the time course of the hydrolysis reaction (data not shown). The observed first-order rate constant fit to the data has a value of $2.1 \times 10^{-4}$ s$^{-1}$, which is similar to that measured by steady-state intensity measurements (Neal et al., 1990; Rensland et al., 1991). It also has been reported (Neal et al., 1990) that no change in the steady state occurs between the mantGTP and mantGDP bound to [Asp-12]-p21$^{N\text{-}ras}$, and the lifetime measurements shown in Table II agree with this.

*Rotational Correlation Times.* Dynamic polarization measurements were carried out on the free and p21-bound mantGDP, mantGTP, and mantdGTP. The steady-state limiting anisotropy for the free mant nucleotide probes was determined independently in 95% glycerol at −10 °C and fixed at 0.37 in the free probe analyses to increase the accuracy and precision of the resolved rotational correlation times. Data taken on free nucleotide derivatives mantGTP, mantdGTP, and mantGDP were fit to single rotational correlation times of 0.34, 0.32, and 0.31 ns, respectively (Table III).

A two-component, exponential decay model was found to give the best fit of the differential phase and modulation data on the p21·nucleotide complexes. The observed rates included a slow rotational correlation time, consistent with the values expected for the slow global tumbling of a protein or protein complex, and a second, faster rotational correlation time, presumably due to either the probe's local motion within the binding site or the structural motion of the surrounding protein domain. The fast motion was not ascribed to free nucleotide since a 4.1-ns lifetime component, corresponding to free mant probe, was not present and gel filtration chromatography after the experiments did not indicate the presence of free probe.

Within experimental error, the three p21$^{ras}$ proteins gave similar global rotational rates with resolved rotational correlation times between 24 and 27 ns with both mantGTP and mantGDP (Table III). The error in the p21$^{K\text{-}ras}$ and p21$^{H\text{-}ras}$ was somewhat higher, although the preparation and handling were similar. The p21$^{N\text{-}ras}$ results were consistent from preparation to preparation, and a representative data set analysis is reported. It should also be noted that the resolved rotational correlation times did not vary across the 1–15 $\mu$M concentration range used in this study.

In all of the mant nucleotide and p21 complexes, the amplitude of the global motion, $r_1$, represented over 92% of the samples' total anisotropy amplitude, $r_1 + r_2$, indicating that the mant fluorophore is held rigidly with little local freedom. The generally poor precision of the observed fast motion is primarily due to the low amplitude, $r_2$, which reflects the fraction of information on this local motion in the decay signal. Thus, the apparent differences in the fast motion of the normal p21$^{N\text{-}ras}$ and Asp-12 oncogenic mutant are uncertain. The use of greater modulation frequencies than those examined here may help increase precision in the data so that these fast motions can be accurately determined.

The theoretical estimates of the rotational correlation times ($\tau_c$) at 5 °C for the p21$^{ras}$ proteins are 15.6 ns for a monomer and 31.2 ns for a dimer, as shown in Table III. These theoretical values are calculated by using the Stoke's–Einstein relationship (for rotation of a spherical body):

$$\tau_c = \frac{M(\bar{v} + \delta)\eta}{RT} \qquad (6)$$

where $R$ is the gas constant, $T$ is the temperature, $v$ is the specific volume of the protein, $\delta$ is the protein's hydration state, and $M$ is the molecular mass. The theoretical rotational correlation time for the p21$^{ras}$ protein was calculated using a monomer molecular mass of 21 kDa, a specific volume of 0.733 cm$^3$/g, calculated from the amino acid analysis (Cohn et al., 1934; McMeekin et al., 1949), and a hydration state of 0.4 g of $H_2O$/g of protein, also calculated from the amino acid analysis (Kuntz, 1971). Equation 6 clearly indicates that the protein rotational correlation time should change in a predictable manner with temperature. Table IV gives the resolved rotational correlation times for p21$^{N\text{-}ras}$·mantGDP at several temperatures, along with the theoretical estimates. The rotational correlation times of p21$^{N\text{-}ras}$·mantGDP decrease with increasing temperature, as would be expected for a normal hydrodynamic particle. All solutions contained 10 mM DTT to disrupt any interprotein disulfide bridges and, hence, remove any possibility that disulfide cross-links could lead to dimers. Furthermore, addition of dithiothreitol to 100 mM had no effect on the resolved rotational correlation times (data not shown).

In highly asymmetric proteins, the fluorophore's orientation along the long or short protein axis can have a considerable effect on the observed rotational correlation time (Beechem et al., 1986; Jameson et al., 1992). The use of multiple fluorescence probes can reduce the likelihood of a particular probe alignment favoring one axis disproportionately. Thus, to investigate further the size and shape characteristics of the p21 proteins and to verify the mant nucleotide results, two additional fluorescent nucleotide derivatives were examined: aminocoumarin GTP and fluorescein GDP. The fluorescence lifetimes of these nucleotide derivatives remained relatively unchanged in their free and bound forms. In solution at 5 °C, aminocoumarin GTP and fluorescein GDP gave single-exponential decays of 3.2 and 3.9 ns, respectively. When bound to p21$^{N\text{-}ras}$ (5 °C), the aminocoumarin GTP lifetime remained unchanged while the fluorescein GDP became heterogeneous, containing both a 4.1-ns lifetime (92% of the intensity) and a 1.2-ns lifetime. Dynamic polarization data were taken, under identical conditions and instrument settings, on p21$^{N\text{-}ras}$·fluorescein GDP, p21$^{N\text{-}ras}$·mantGDP, and p21$^{N\text{-}ras}$·aminocoumarin GTP. Data were analyzed individually and coanalyzed, linking the global rotational correlation time function, using the Globals Unlimited analysis software. The global analysis best fit to the differential phase and modulation data of all three complexes is shown in Figure 3A (modulation data not shown), and the $\chi^2$ map of the linked parameter, $\tau_{c1}$, is given in Figure 3B. The overall protein rotational rate from the linked analysis was 28 ns. A summary of the rotational parameters from the global and single analyses is given in Table V. Local rotational modes of the attached fluorophores, $\tau_{c2}$, and the associated anisotropy amplitudes,

Table III: Rotational Parameters (5 °C)

| sample[a] | $\tau_{c1}$ (ns) | $r_1$ | $\tau_{c2}$ (ns) | $r_2$ | $\chi^2$ |
|---|---|---|---|---|---|
| mantGDP | 0.31 ± 0.01 | 0.37[b] | | | 3.6 |
| mantGTP | 0.34 ± 0.01 | 0.37[b] | | | 3.8 |
| mantdGTP | 0.32 ± 0.04 | 0.37[b] | | | 3.0 |
| $p21^{N\text{-}ras}$·mantGDP | 25 ± 1 | 0.34 ± 0.01 | 1.3 ± 0.7 | 0.03 ± 0.01 | 0.9 |
| [$Asp^{12}$]$p21^{N\text{-}ras}$·mantGDP | 26 ± 1 | 0.34 ± 0.00 | 0.2 ± 0.1 | 0.03[c] | 1.0 |
| $p21^{H\text{-}ras}$·mantGDP | 27 ± 3 | 0.31 ± 0.01 | 0.6 ± 0.5 | 0.07 ± 0.03 | 3.5 |
| $p21^{K\text{-}ras}$·mantGDP | 24 ± 5 | 0.32 ± 0.04 | 0.1 ± 0.1 | 0.02 ± 0.03 | 3.8 |
| $p21^{N\text{-}ras}$·mantGTP | 26 ± 1 | 0.35 ± 0.02 | 1.4 ± 0.6 | 0.02 ± 0.01 | 0.5 |
| [$Asp^{12}$]$p21^{N\text{-}ras}$·mantGTP | 26 ± 1 | 0.35 ± 0.00 | 0.6 ± 0.7 | 0.03 ± 0.04 | 0.7 |
| $p21^{N\text{-}ras}$·mantdGTP | 23 ± 1 | 0.34 ± 0.01 | 1.5 ± 0.7 | 0.03 ± 0.00 | 0.8 |
| theoretical values[d] | | | | | |
| monomer | 15.6 | | | | |
| dimer | 31.2 | | | | |

[a] Representative data sets are shown for the $p21^{N\text{-}ras}$ samples. The reported $p21^{H\text{-}ras}$ and $p21^{K\text{-}ras}$ results are averages of three separate data sets. Errors represent the standard deviation estimated within the least-squares fitting procedure. [b] Independently determined at −10 °C in 95% glycerol and fixed in the analysis. [c] The limiting anisotropy, the sum of $r_1$ and $r_2$, was fixed at 0.37, and thus only one standard error is obtained. [d] Estimates of the rotational correlation times were calculated for a spherical protein as detailed in the text.

Table IV: $p21^{N\text{-}ras}$·mantGDP Temperature Dependence of $\tau_{c1}$

| sample temp (°C) | $\tau_{c1}$ (ns) observed | $\tau_{c1}$ (ns) theory[a] |
|---|---|---|
| 30.3 | 10.4 | 7.5 |
| 20.6 | 14.3 | 9.8 |
| 14.5 | 17.4 | 11.3 |
| 10.7 | 20.9 | 13.2 |
| 4.9 | 24.4 | 15.6 |

[a] Theoretical estimates of the rotational correlation times were calculated for a spherical protein.

$r_2$, were also resolved for the three samples. The local motion amplitudes for $p21^{N\text{-}ras}$·mantGDP, $p21^{N\text{-}ras}$·coumarin GTP, and fluorescein GDP complexes were 0.00, 0.06, and 0.14, respectively. The observed increase in the amplitude correlates with an increasing fluorophore spacer length (see Figure 1), as one might predict.

*Analytical Gel Permeation Chromatography.* Estimates of the molecular size of the $p21^{N\text{-}ras}$·GDP and $p21^{N\text{-}ras}$·mantGDP complexes were measured using analytical gel permeation chromatography on an ACA-54 column. The $p21^{N\text{-}ras}$·GDP and $p21^{N\text{-}ras}$·mantGDP complexes ran as a single peak with apparent molecular masses and standard deviations (derived from the standard curve) of 27 ± 3 and 28 ± 3 kDa, respectively. The complexes gave similar results, alleviating concerns of a mant-induced dimerization, with values 30% higher than the expected 21 kDa, as determined from the sequence. Rotational correlation times (taken at 5 °C) for $p21^{N\text{-}ras}$·mantGDP were 25.5 ns before and 24.4 ns after gel filtration, ruling out the possibility of column- or time-induced artifacts.

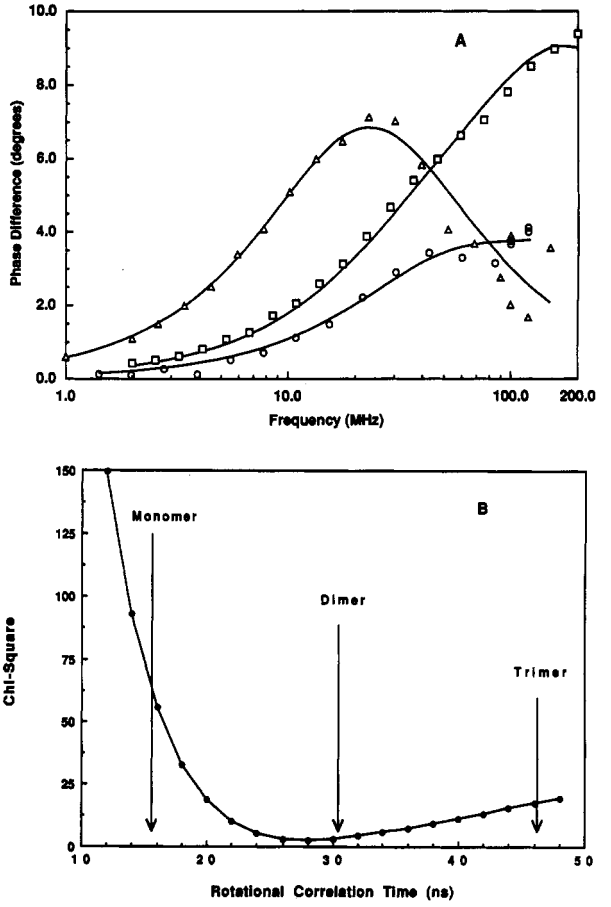


FIGURE 3: (A) Dynamic polarization phase (—) data for $p21^{N\text{-}ras}$·mantGDP (△), $p21^{N\text{-}ras}$·fluorescein GDP (□), and $p21^{N\text{-}ras}$·aminocoumarin GTP (○) at 5 °C. The mantGDP and aminocoumarin GTP samples were excited with the 351-nm line of an argon ion laser, and emission was measured through Schott GG 420 and KV 399 cutoff filters. The fluorescein-containing samples were excited at the 488-nm argon ion laser line, and emission was monitored through a Schott OG 530 cutoff filter. The curves represent the least-squares best fits to the data by the global analysis routines in which all three data sets were simultaneously fit while minimizing the aggregate $\chi^2$ (data in Table V). (B) The $p21^{N\text{-}ras}$ $\chi^2$ minimization map of the globally fit protein rotational correlation time, $\tau_{c1}$. Arrows indicate the expected values for a spherical monomer, dimer, and trimer $p21^{N\text{-}ras}$ protein.

## DISCUSSION

Fluorescence lifetime and fluorescence dynamic polarization measurements can address the solution hydrodynamics of macromolecules under equilibrium conditions. For a fluorescent probe bound to a unique site, such as the fluorescent nucleotide derivatives used here, information on the local conformational changes in the region of the probe can also be monitored. The mant nucleotide probes are covalently attached at the 2′ or 3′ position of the nucleotide ribose ring and are thus well-positioned to monitor conformational changes in the $p21^{ras}$ nucleotide site. As shown, a large fluorescence lifetime change was observed, from 4 to 9 ns, when the mant nucleotide probes bound to any of the p21 proteins. The fact that the addition of excess unlabeled GDP displaces mantGDP from the binding site verifies the specific binding of the mant analogues to the nucleotide site.

Table V: p21$^{N\text{-}ras}$ Global Analyses (5 °C)

| sample | $\tau_{c1}$ (ns) | $r_1$ | $\tau_{c2}$ (ns) | $r_2$ | $\chi^2$ |
|---|---|---|---|---|---|
| | | Individual Analyses | | | |
| p21$^{N\text{-}ras}$·mantGDP | 28 ± 1 | 0.36 ± 0.01 | 0.0 | 0.00 | 5.8 |
| p21$^{N\text{-}ras}$·coumarin GTP | 29 ± 3 | 0.34 ± 0.01 | 0.4 ± 0.6 | 0.05 ± 0.04 | 0.9 |
| p21$^{N\text{-}ras}$·fluorescein GDP | 19 ± 1 | 0.22 ± 0.00 | 0.8 ± 0.7 | 0.13 ± 0.00 | 0.2 |
| | | Globally Linked Analysis | | | |
| p21$^{N\text{-}ras}$·mantGDP | 28[a] | 0.37 | 0.0 | 0.00 | 5.9 (local) |
| p21$^{N\text{-}ras}$·coumarin GTP | 28[a] | 0.34 | 0.3 | 0.06 | 0.9 (local) |
| p21$^{N\text{-}ras}$·fluorescein GDP | 28[a] | 0.21 | 1.1 | 0.14 | 0.8 (local)<br>2.6 (global) |

[a] The global motion of the p21$^{N\text{-}ras}$ species, $\tau_{c1}$, was linked in the analysis.

mant nucleotides exist free in solution at pH 7.5 as an equilibrium mixture of the 2′-*O* and 3′-*O* derivatives in a ratio of approximately 40:60 and a reaction half-time of approximately 7 min (Cremo et al., 1990; Rensland et al., 1991; Eccleston et al., 1991). The fluorescence intensity of the two isomers differs by a factor of 2 and thus potentially complicates the time-resolved fluorescence measurements reported here. However, no differences in behavior were detected between mantGTP and mantdGTP, where the mant group is fixed to the 3′-*O* position. This observation is consistent with the previous data in which it was shown that the binding of the equilibrium mixture to p21$^{ras}$ results in the predominant binding of the 3′-*O* isomer and that the ratio of the two isomers does not change during the time course of the hydrolysis of mantGTP.

Local conformational differences between the GTP and GDP forms of p21$^{ras}$ proteins have been primary focal points in much p21$^{ras}$ research. Pertinent studies reported in the literature include the use of NMR, CD, and X-ray crystallography, all of which have noted shifts in the GTP and GDP conformational forms and among the normal and mutant ras proteins (Pingoud et al., 1988; Campbell-Burke et al., 1989; Schlichting et al., 1990a,b). The most detailed information has been supplied by comparisons of crystal structures on the truncated p21$^{H\text{-}ras}$ bound with GTP, GDP, and Gpp[NH]p (Pai et al., 1989; Schlichting et al., 1990a; Pai et al., 1990; Milburn et al., 1990). Steady-state fluorescence spectra of the p21$^{N\text{-}ras}$·mantGTP and p21$^{N\text{-}ras}$·mantGDP complexes previously reported indicated a 10% increase in fluorescence intensity of the GTP form over the GDP form (Neal et al., 1990). The lifetime data collected at 5 °C indicate a 2% increase in the lifetime value of the GTP form relative to the GDP form. In contrast, data collected at 30 °C show a 7.8% increase the mantGTP over the mantGDP p21$^{ras}$ complexes. The observed intensity and lifetime differences could be due to a polarity change in the mant environment or to a change in quenching efficiency by p21-specific residues in p21$^{ras}$·mantGDP compared to p21$^{ras}$·mantGTP. If a quenching effect is responsible, then the fact that the intensity and lifetime data correlate would suggest a primarily dynamic process. In the crystal structures, the Tyr-32 residue is in close proximity to the nucleotide binding site and shows a rather large positional shift between the p21$^{ras}$ GTP and GDP forms; perhaps this alteration is connected with the observed fluorescence changes (Goody et al., 1992).

Related to the local conformational differences between the GTP and GDP forms of the p21$^{ras}$ proteins is the GTP character of the transforming p21 proteins. Steady-state fluorescence data previously reported had indicated a correlation between the transforming ability of a p21$^{ras}$ protein and the absence of a fluorescence intensity difference between the mantGTP and mantGDP complexes of the specific p21 protein (Eccleston et al., 1991). At 5 °C neither the lifetime nor the rotational data indicated significant differences between the mantGTP or the mantGDP complexes of the normal p21$^{N\text{-}ras}$ and the [Asp-12]p21$^{N\text{-}ras}$ oncogenic mutant. This was not the case at 30 °C where the fluorescence lifetime dropped by 7.8% between the mantGTP and mantGDP forms of the normal protein. The Asp-12 mutant had virtually the same lifetime for both nucleotide conformations, indicating a loss of the GTP to GDP conformational shift monitored with the mant probe. If the Asp-12 mutant indeed retains a similar conformation in both the GTP and GDP forms, then this character must define the transformation ability of the mutant.

The primary question on which our dynamic polarization data has bearing concerns the molecular size and shape of the p21$^{ras}$ proteins. The resolved rotational correlation times for the *N-ras*, *K-ras*, and *H-ras* full-length p21 proteins at 5 °C complexed with mant nucleotide probes were between 24 and 28 ns (Table III). The calculated (outlined in the Results) rotational correlation time for a hydrated, monomeric protein with a molecular mass of 21 kDa at 5 °C is 15.6 ns. The disparity between the estimate and the resolved value is significant. The results suggest two possibilities: either the p21$^{ras}$ proteins exist as dimers, or the spherical shape suggested by the X-ray crystal structures is not an accurate representation of the fully hydrated solution structure for these proteins.

Preliminary to our discussion on the possible shape or oligomeric nature of p21$^{ras}$ is some consideration of the theoretical estimate of the p21 rotational correlation time. We are not concerned with the mathematical approach to the rotation of ellipsoids in solution, which is well established, but with the major assumptions in the theoretical calculations that are less defined and more protein-specific, namely, the protein specific volume and the hydration state. An estimate of specific volume can be obtained from the amino acid analysis (Cohn et al., 1934). This approach sums the specific volume of each amino acid to give an approximate specific volume for the protein in question. Specific volumes for proteins range from 0.69 and 0.75 cm$^3$/g with a value calculated for p21 of 0.733 cm$^3$/g. In order to account for the observed rotational correlation time of p21 with a monomeric, spherical protein, eq 6 would require the unacceptably large specific volume of 1.5 cm$^3$/g. Assuming the largest value of the normal range of specific volumes mentioned above, one would only see a 1–2% increase in the estimated rotational correlation time. This parameter, then, does not appear to be a source for any significant error.

The hydration state, like the protein's specific volume, helps to determine the apparent volume of a protein in solution and as such influences the estimate of the rotational correlation time. However, the hydration state of a protein and, for that matter, the effect of the hydration state on the observed

hydrodynamic parameters such as the translational and rotational correlation times are not fully understood. Various methods have been used to estimate the amount of bound water in a hydrated protein: values have generally been between 0.2 and 0.5 $cm^3$ of $H_2O$/g of protein for soluble proteins. Here, we have estimated the p21 hydration state at 0.4 $cm^3$/g by summing the hydration for each amino acid and assuming that each is fully hydrated (Kuntz, 1971). A comparison of the calculated protein hydration state with experimental values indicates that the calculated value agrees with or slightly over estimates the amount of bound water [see Kuntz (1971) and Cantor and Schimmel (1980)]. In order to account for the observed rotational correlation time of 26 ns with a $p21^{ras}$ monomer, one would have to assume a hydration state of 1.2 $cm^3$ of $H_2O$/g of protein. This result is several times the measured value for proteins and is difficult to justify.

If we thus consider that the theoretical rotational correlation times are reasonable, we must then assume that the large discrepancy between the observed and calculated values is significant and is due to the particular solution behavior of the $p21^{ras}$ proteins. The most straightforward explanation of our data would be the presence of a dimeric $p21^{ras}$ protein. Support for this hypothesis exists in the literature. A number of ras homologues have been identified in solution as oligomers (Kawata, 1988; Ueda et al., 1990; Arakai et al., 1990; Mizuno et al., 1991), and evidence has been presented by Santos and co-workers (Santos et al., 1988) using neutron inactivation methodologies. In addition, gel permeation chromatography by John et al. (1989) and repeated here gives a 20–30% increase in the apparent molecular mass from the expected 21 kDa. These results support the possibility of interactions between monomer $p21^{ras}$ proteins.

Several observations, however, do not coincide with the oligomer hypothesis. NMR data on the p21 proteins, under conditions where the cysteines are fully reduced, suggest a primarily monomeric enzyme. The presence of 42-kDa p21 dimers would render NMR line widths exceptionally broad and the peak assignments less clear than what is observed (S. Campbell-Burke, personal communication). However, a fast equilibrium between the monomer and dimer states or substantial protein structural motion could compensate for the dimer-induced line broadening. Secondly, the reported crystal structures of truncated $p21^{H\text{-}ras}$ show a p21 monomer as the asymmetric unit, uncharacteristic of dimeric proteins. Gel permeation chromatography indicates only a 20–30% increase in the apparent size and an unconvincing dimer molecular mass. Lastly, from sedimentation data Pingoud and co-workers determined a Svedberg coefficient of 2.4 S for full-length $p21^{H\text{-}ras}$ (Pingoud et al., 1988), which matches the expected value for a hydrated, spherical monomer. The reported data, then, on the p21 oligomeric state are mixed, with the overall sense that the $p21^{ras}$ proteins have a tendency to aggregate.

Traditional evidence for a monomer–dimer system usually consists of a concentration-dependent change in apparent size. Our results show no such change in the protein rotational correlation time over the 1–15 $\mu$M concentration range examined and thus require that the dissociation constant be below micromolar. Limitations in the dynamic polarization technique, which stem from the instrument and the properties of the particular fluorophore, prohibited the use of $p21^{ras}$ concentrations much below 1 $\mu$M. These concentrations, however, are comparable to the 1.6–6.3 $\mu$M used in the inactivation experiments (Santos et al., 1988) and to the gel filtration experiments reported here. Reports on $p21^{ras}$ using NMR, ultracentrifugation (Pingoud et al., 1988), and gel filtration (John et al., 1989) applied significantly higher protein concentrations than those in this report and would have been expected to contain the postulated dimer.

A second hypothesis, which would also be consistent with our data, is that the $p21^{ras}$ proteins have an elongated shape, giving rise to increased rotational correlation times. Fluorescence polarization measurements are more sensitive to the shape of a protein than the other hydrodynamic techniques, such as gel filtration or ultracentrifugation. Examination of the crystal structures indicates that the dimensions of the p21 proteins are globular with approximate axial distances of 35 × 40× 49 Å. Equations describing the expected rotational correlation times for a general ellipsoid have been published (Perrin, 1934; Small et al., 1988) that, when given the above dimensions, cannot account for the rotational correlation times observed, assuming a monomeric protein. In fact for the monomer, the largest expected correlation time, for any probe orientation for a protein with these dimensions, is only 11% larger than that estimated for the equivalent sphere. It is not clear how much one can rely on the crystal structure data to accurately represent the overall solution shape of these proteins. All of the reported crystal structures were determined on truncated $p21^{ras}$ proteins, not the full-length protein. In order to explain our data in terms of the shape of a monomeric p21 protein, a more extended structure must be invoked. A prolate ellipsoid with a minimum axial ratio of 2.5:1 would be consistent with the dynamic polarization data presented herein. If a protein is truly spherical in shape, then the resolved rotational correlation time would be independent of probe orientation. The rotational results on the fluorescein GDP (individual analysis, Table V) appear to be somewhat disparate with the other two probes. It could be that the fluorescein GDP actually monitors a faster rotational correlation time along a specific ellipsoidal axis, as described above. Alternatively, this result could be consistent with the existence of a dimer in which the fluorescein moiety can undergo self energy transfer, leading to depolarization.

The data herein do not differentiate between the two interpretations of the protein rotational data presented. Clearly, the fluorescence data indicate some physical property of the p21 solution structure not clearly observed in other techniques. Since the present focus on the mechanism of p21 GTP hydrolysis centers on conformational changes between the GTP- and GDP-bound states and the possibility of an isomerization of the $p21^{ras}$·mantGTP complex preceding hydrolysis (Neal et al., 1990), the understanding of the solution behavior is relevant. The formation or reorganization of dimer complexes may be important in the GTPase mechanism of $p21^{ras}$ and may represent a modulating factor in the hydrolysis mechanism.

If $p21^{ras}$ can form dimers, then whether $p21^{ras}$ acts physiologically as a dimer or monomer will be dependent on the protein's local concentration within the cell. Total cellular concentrations have been estimated to be between 10 and 100 nM (Muller et al., 1992), but these values are likely to be lower than the actual local concentrations that will determine the extent of dimerization. With the present ambiguities, it is not yet possible to estimate the extent of dimerization *in vivo*. Along these lines, it will also be of interest to establish whether dimerization of $p21^{ras}$ plays a role in defining its interactions with putative protein effectors: $p21^{ras}$ GAP (Trahey & McCormick, 1987), neurofibromin (Xu et al., 1990), and nucleotide exchange factors (Downward et al.,

1990). Evidence on a number of ras-like proteins suggests the formation of heterodimers with these effectors, which suggests the possibility of a competition between heterodimer and homodimer as a possible regulation of ras activity. Clearly, further data on the physical state of the p21 proteins are needed before we can fully understand the solution structure of these proteins and how this structure influences the association of their upstream or downstream effectors.

## ACKNOWLEDGMENT

We thank Dr. J. E. T. Corrie for the gift of aminocoumarin.

## REFERENCES

Arakai, S., Kikuchi, A., Hata, Y., Isomura, M., & Takai, Y. (1990) *J. Biol. Chem. 265*, 13007–13015.
Barbacid, M. (1987) *Annu. Rev. Biochem. 56*, 779–827.
Beechem, J. M., Knutson, J. R., & Brand, L. (1986) *Biochem. Soc. Trans. 14*, 832–835.
Bourne, H. R., Sanders, D. A., & McCormick, F. (1990) *Nature 348*, 125–132.
Campbell-Burke, S., Papastavros, M. Z., McCormick, F., & Redfield, A. G. (1989) *Proc. Natl. Acad. Sci. U.S.A. 86*, 817–820.
Cantor, C. R., & Schimmel, P. R., Eds. (1980) *Biophysical Chemistry*, W. H. Freeman and Company, San Francisco, CA.
Chen, R. F. (1969) *Arch. Biochem. Biophys. 133*, 263–276.
Cohn, E. J., McMeekin, T. L., Edsall, J. T., & Blanchard, M. H. (1934) *J. Am. Chem. Soc. 56*, 784–794.
Corrie, J. E. T. (1990) *J. Chem. Soc., Perkin Trans. 1*, 2151–2152.
Cremo, C. R., Neuron, J. M., & Yount, R. G. (1990) *Biochemistry 29*, 3309–3319.
Downward, J., Riehl, R., Wu, L., & Weinberg, R. A. (1990) *Proc. Natl. Acad. Sci. U.S.A. 87*, 5998–6002.
Eccleston, J. F., Moore, K. J. M., Brownbridge, G. G., Webb, M. R., & Lowe, P. N. (1991) *Biochem. Soc. Trans. 19*, 432–436.
Feuerstein, J., Goody, R. S., & Wittinghofer, A. (1987) *J. Biol. Chem. 262*, 8455–8458.
Goody, R. S., Pai, E. F., Schlichting, I., Rensland, H., Scheidig, A., Franken, S., & Wittinghofer, A. (1992) *Phil. Trans. R. Soc. London B 336*, 3–11.
Gratton, E., & Limkeman, M. (1983) *Biophys. J. 44*, 315–324.
Gratton, E., Jameson, D. M., & Hall, R. D. (1984) *Annu. Rev. Biophys. Bioeng. 13*, 105–124.
Hall, A. (1990) *Science 249*, 635–640.
Hall, A., & Self, A. (1986) *J. Biol. Chem. 262*, 8455–8458.
Hiratsuka, T. (1983) *Biochim. Biophys. Acta 742*, 496–508.
Jameson, D. M., & Hazlett, T. L. (1991) in *Biophysical and Biochemical Aspects of Fluorescence Spectroscopy* (Dewey, G., Ed.) pp 105–133, Plenum Press, New York.
Jameson, D. M., Gratton, E., & Hall, R. D. (1984) *Appl. Spectrosc. Rev. 20*, 55–106.
Jameson, D. M.,Brunet, J. E., Vargas, V., & Gratton, E. (1992) *Biophys. J. 61*, A310.
John, J., Schlichting, I., Schiltz, E., Rosch, P., & Wittinghofer, A. (1989) *J. Biol. Chem. 264*, 13086–13092.
John, J., Sohmen, R., Feuerstein, J., Linke, R., Wittinghofer, A., & Goody, R. S. (1990) *Biochemistry 29*, 6058–6065.
Kawamura, S., Kaibuchi, K., Hiroyoshi, M., Hata, Y., & Takai, Y. (1991) *Biochem. Biophys. Res. Commun. 174*, 1095–1102.
Kawata, M. (1988) *J. Biol. Chem. 263*, 18965–18971.
Kuntz, I. D. (1971) *J. Am. Chem. Soc. 93*, 514–518.
Lowe, P. N., Page, M. J., Bradley, S., Rhodes, S., Sydenham, M., Paterson, H., & Skinner, R. H. (1991) *J. Biol. Chem. 266*, 1672–1678.
Maeda, M., Patel, A. D., & Hampton, A. (1977) *Nucleic Acids Res. 4*, 2843–2853.
McMeekin, T. L., Groves, M. L., & Hipp, N. J. (1949) *J. Am. Chem. Soc. 71*, 3298–3300.
Milburn, M. V., Tong, L., DeVos, A. M., Brunger, A., Yamaizumi, Z., Nishimura, S., & Kim, S.-H. (1990) *Science 247*, 939–945.
Mizuno, T., Kaibuchi, K., Yamamoto, Y., Kawamura, M., Sakoda, T., Fujioka, H., Matsuura, Y., & Takai, Y. (1991) *Proc. Natl. Acad. Sci. U.S.A. 88*, 6442–6446.
Muller, O., Frech, M., Gideon, P., Wittinghofer, A. W., & Schwartz, M. (1992) *Oncogene 7*, 1407–1412.
Neal, S. E., Eccleston, J. F., & Webb, M. R. (1990) *Proc. Natl. Acad. Sci. U.S.A. 87*, 3562–3565.
Pai, E. F., Kabsch, W., Krengel, U., Holmes, K. C., John, J., & Wittinghofer, A. (1989) *Nature 341*, 209–214.
Pai, E. F., Krengel, U., Petsko, G. A., Goody, R. S., Kabsch, W., & Wittinghofer, A. (1990) *EMBO J. 9*, 2351–2359.
Perrin, F. (1934) *J. Phys. Rad. (Ser. VII) 5*, 487–511.
Pingoud, A., Wehrmann, M., Pieper, U., Gast, F.-U., Urbanke, C., Alves, J., Feuerstein, J., & Wittinghofer, A. (1988) *Biochemistry 27*, 4735–4740.
Rensland, H., Lautwein, A., Wittinghofer, A., & Goody, R. S. (1991) *Biochemistry 30*, 11181–11185.
Santos, E., Nebreda, A. R., Bryan, T., & Kempner, E. S. (1988) *J. Biol. Chem. 263*, 9853–9858.
Schlichting, I., Almo, S. C., Rapp, G., Wilson, K., Petratos, K., Lentfer, A., Wittinghofer, A., Kabsch, W., Pai, E. F., Petsko, G. A., & Goody, R. S. (1990a) *Nature 345*, 309–315.
Schlichting, I., John, J., Frech, M., Chardin, P., Wittinghofer, A., Zimmermann, H., & Rosch, P. (1990b) *Biochemistry 29*, 504–511.
Small, E. W., Libertini, L. J., & Small, J. R. (1988) *Proc. SPIE 909*, 97–107.
Spencer, R. D., & Weber, G. (1969) *Ann. N.Y. Acad. Sci. 158*, 361–376.
Spencer, R. D., & Weber, G. (1970) *J. Chem. Phys. 52*, 1654–1663.
Tong, L., deVos, A. M., Milburn, M. V., Jancarik, J., Noguchi, S., Nishimura, S., Miura, K., Ohtsuka, E., & Kim, S.-H. (1989) *Nature 337*, 90–93.
Tong, L., Milburn, M. V., deVos, A. M., & Kim, S.-H. (1990) *Science 245*, 244.
Trahey, M., & McCormick, F. (1987) *Science 238*, 542–545.
Ueda, T., Kikuchi, A., Ohga, N., Yamamoto, J., & Takai, Y. (1990) *J. Biol. Chem. 265*, 9373–9380.
Weber, G. (1977) *J. Chem. Phys. 66*, 4081–4091.
Weber, G. (1981) *J. Phys. Chem. 85*, 949–953.
Wittinghofer, A., Krengel, U., John, J., Kabsch, W., & Pai, E. F. (1991) *Environ. Health. Perspect. 93*, 11–15.
Xu, G., O'Connell, P., Viskochil, D., Cawthorn, R., Robertson, M., Cluver, M., Dunn, D., Stevens, J., Gesteland, R., White, R., & Weiss, R. (1990) *Cell 62*, 599–608.